Plug-and-Play Nonlinear Droop Construction Scheme to Optimize Islanded Microgrid Operations

Fatih Cingoz, *Student Member, IEEE*, Ali Elrayyah, *Member, IEEE*, and Yilmaz Sozer, *Senior Member, IEEE*

***Abstract*—The operating cost of islanded microgrids (μGs) can be minimized by performing an optimal power sharing among the distributed generators (DGs). In this study, a plug-and-play optimization scheme (PPOS) for developing nonlinear droop relations is proposed to achieve an optimal power sharing among DGs in islanded μGs. The PPOS constructs optimal nonlinear relations for each DG, which are used as nonlinear droop curves that adjusts the output power of the DGs subsequent to any load variation to minimize the μG operating cost effectively. The construction of nonlinear droop relations in the PPOS is performed individually for each DG by optimizing each one against hypothetical DGs. This approach provides an indirect optimization among different DGs in the μG network and ensures an operating cost minimization irrespective of the μG topology. An islanded μG topology has been developed and simulated in MATLAB/Simulink environment to verify the effectiveness of the proposed method and the performance of the nonlinear droop control. An experimental study has also been conducted on a μG test bed to prove the effectiveness of the nonlinear power sharing and to verify the performance of the nonlinear droop control in the μG operating cost minimization.**

***Index Terms*—Microgrids, nonlinear droop control, plug-and-play optimization.**

I. Introduction

THE rapid development in global industry and economy increased the world demand for energy in the last two decades and in the future as well, e.g., 85% increase in energy consumption is projected in coming three decades by U.S. Energy Information Administration (EIA) [1]. Conventional energy sources, particularly fossil fuel based, have introduced a satisfactory response to energy demand growth. However, environmental pollution and global warming became inevitable threats due to continuous increase in greenhouse gas emissions. The growth in the demand in addition to different environmental and economic concerns have motivated researchers to consider the adoption of installing alternative energy sources integrated in a distributed fashion, and thus, they are called distributed generators (DGs).The notion of distributed generation supports improved power quality [2], reliability [2]–[4], stability [5], efficiency [6]–[9], and expandability [10] compared to centralized generation. These advantages are better realized through microgrids (μGs) in which DGs, loads and energy-storage units are effectively integrated together at distributed voltage level [6]–[9]. Microgrids are defined as controllable small-scale power networks that can operate either in grid-tied or islanded operation modes.

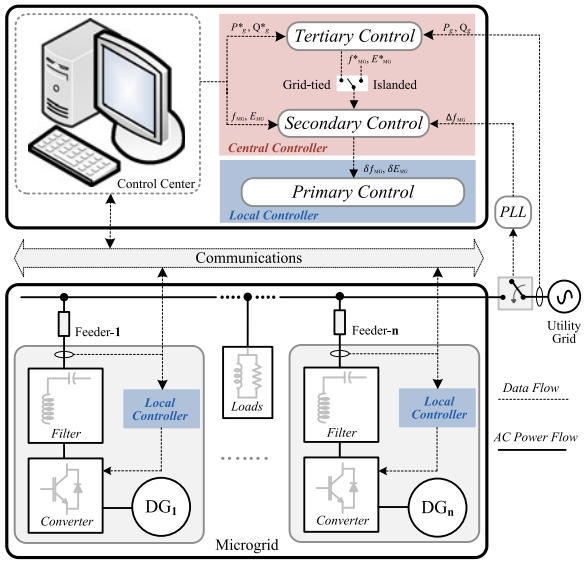

Fig. 1. General psychical configuration and control hierarchy of a μG.

Having various DGs with different properties connected to the same distribution system differentiates the μGs from the conventional central power networks. Many types of DGs (e.g., IC-engine generators, microturbines, and fuel cells) with power rating that is in the range of few kilowatts up to megawatts can be interfaced with the μGs network through power electronic inverters. Inverter based μGs introduce higher operation flexibility and controllability compared to conventional power systems. However, inverter-based sources have low inertia, making the μGs more sensitive to network disturbances in contrast to the traditional power networks [11], [12]. Furthermore, the intermittent nature of renewable type DGs (e.g., wind turbines, photovoltaic panels) in μGs complicates the power management and may jeopardize their stability [12]. Accordingly, different control structures have been developed to achieve stable and cost-effective μG operation [9], [13]–[19]. A structural control system for μGs has been recently introduced where such a system consists of three main control levels, namely, the primary, the secondary, and the tertiary [11], [20]. Fig. 1 shows the overall μG configuration and control levels in the hierarchical structure.

The μG dynamics such as frequency and bus voltage are mainly dictated by the utility grid in grid-tied mode operation.

Manuscript received July 14, 2015; revised October 9, 2015, December 29, 2015, and March 7, 2016; accepted April 18, 2016. Date of publication May 27, 2016; date of current version January 20, 2017. Recommended for publication by Associate Editor V. Agarwal.

F. Cingoz and Y. Sozer are with the Electrical and Computer Engineering Department, University of Akron, Akron, OH 44325 USA (e-mail: fc17@zips.uakron.edu; ys@uakron.edu).

A. Elrayyah was with the Electrical and Computer Engineering Department, University of Akron, Akron, OH 44325 USA. He is now with the Qatar Environment and Energy Research Institute, Doha 5825 Qatar (e-mail: aelrayyah@qf.org.qa).

Color versions of one or more of the figures in this paper are available online at http://ieeexplore.ieee.org.

Digital Object Identifier 10.1109/TPEL.2016.2574202

However, in case of islanded μGs, its dynamics are greatly influenced by the DGs and their power management and control systems [11], [20]. In the islanded μGs, any power mismatch may lead to voltage and frequency instability. Thus, the primary control, which is the first and most significant control level in Fig. 1, is essentially designed to stabilize the frequency and voltage in the islanded μGs while providing autonomous load sharing among DGs. In addition, the primary control terminates undesired circulating currents autonomously without the need of an explicit communication system [11], [20]. On the other hand, the secondary control is particularly employed to compensate for the frequency and voltage deviations produced by the local control loops in the primary control level. This task is required to realize the synchronization between the islanded μG with the utility grid whenever needed. As a last control level, the tertiary control level regulates the power flow between the μG and the utility grid to achieve an economical operation in grid-tied μGs [11]. However, in the islanded μGs, the main objective as explained before has been to provide autonomous power sharing among DGs proportional to their power ratings. To carry out such power sharing, linear droop control technique has been effectively utilized as a local controller in the primary control level. It will be shown in this paper that although this droop control technique has the advantages of simplicity, reliability and flexibility, the islanded μG operating cost may not be optimized effectively due to variety and nonlinearity in the relation between the produced power and the operation cost of the various DGs. To address the issue of cost-effective islanded μG operation, different droop techniques have been studied in the literature [21]–[29]. In [21], dynamic droop control has been proposed to optimize the power sharing among the DGs and accordingly, minimize the overall fuel consumption in the islanded μGs. Despite the fact that this type of droop scheme successfully increases the economic benefits, it requires a centralized communication network, which increases the complexity, failure risk, and the cost of the μG [21]. Therefore, several alternative methods have been introduced to provide cost-effective μG operation without the need of communication network [22]–[29]. In [22], a single operating cost function is selected as a reference among the operating cost functions defined for all DGs to determine the values of offset parameters for each DG. Then, these offset values are included into the conventional droop relation to construct a cost-effective nonlinear droop relation for each DG. This method has been further improved in [23] and [24], in which the droop relation of each DG has been formulated based on its associated operating cost function. It has been shown that the nonlinear droop relations formulated by this cost-function-based method (CFB) are better to track the cost variations of the DGs and, thus, introduce improved operating cost reduction. As a solution to complexity and accuracy issues in nonlinear droop relations, maximum and mean cost-based (MCB) methods have been introduced in [25]. Unlike the other methods introduced in [22]–[24], the MCB method formulates cost-effective linear droop relations in which the droop coefficients are determined based on either maximum or mean operating cost values of the DGs. These methods proposed in [22]–[25] are simple and cost effective; however, formulating the droop relations according to the operating cost characteristics of the DGs could be allowed to have a more general shape such that more flexibility in constructing the optimal nonlinear droop relations can be achieved for better cost saving. In [26] and [27], a nonlinear-function-based (NFB) method has been proposed to offer more flexibility in constructing the nonlinear droop relations such that more cost saving in the μG operation can be realized. In this method, the nonlinear droop relations are mathematically defined as a combination of functions where each one is represented by a source power raised to an integer and fractional exponent. Then, the coefficients of the power functions are specified through a heuristic optimization technique called particle swarm optimization (PSO) to construct the optimal nonlinear droop relations for each DG. This method is slightly more complicated, but it provides better nonlinear droop relations to be implemented in droop control and, consequently, leads to improved cost-effective μG operation. However, the optimization problem defined for the NFB method lacks the proper consideration for different constraints, which may result in frequency sensitivity degradation in the μG. In addition, the NFB method forces all the nonlinear droop curves of all DGs to start from one point and end at the same point, which limits the flexibility in constructing the optimal nonlinear droop curves or relations. As the major drawback of the NFB method, any modification in the active DGs requires the entire optimization problem to be redefined and solved again, which incapacitates the plug-and-play capability of the droop control method.

The main target of these methods mentioned above is to formulate optimal droop relations that minimize the total operating cost of the μG system considering that all participating DGs are preferred to be continuously online. There exist other methods proposed in [28] and [29] in which the droop relations are formulated such that DGs with high operating cost are switched off autonomously during light loadings and operated only at high loadings. In [28], the droop relation of each DG is formulated using its associated no-load operating cost value, which gives higher dispatch priorities to the DGs introducing relatively lower no-load operation costs. This method has been further improved in [29] by formulating the droop relations based on several factors rather than only no-load operating cost. Droop relations are constructed using the information of operating costs, number of the DGs, and their power ratings and taking some constraints, i.e., online power reserve, power limits, into account. These methods introduced in [28] and [29] offer considerable cost savings particularly when no loading operating costs are taken into account. This paper focuses on developing a similar method proposed in [22]–[27] to minimize the total operating cost in a μG where the DGs are desired to be operated continuously for all possible loading conditions. In this paper, a new method named as plug-and-play optimization scheme (PPOS) is proposed as an extension of the NFB method to realize a flexible, and a topology independent nonlinear droop relation construction. As the main improvement, the proposed method is aimed to construct the optimal nonlinear droop relations for every DG independently without considering the cost and/or droop relations of the other DGs in the μG network. This is carried out by optimizing each DG against some user-defined

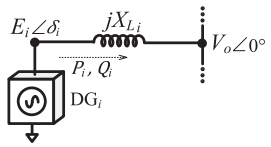

Fig. 2. Equivalent circuit of two DG units connected to μG common bus through inductive lines.

(hypothetical) DGs whose droop relations and operation cost functions are predefined and used as reference. In this way, it is expected that the μG operating cost will be successfully minimized while maintaining the plug-and-play capability of the nonlinear droop control.

The paper is organized as follows. In Section II, the basic concepts of the linear droop and the other proposed droop techniques are discussed in details. Then, the method of the construction of the optimal nonlinear droop relations is introduced in Section III. The PSO and its implementation are also covered in the same section. The basic principles and implementation of the proposed method is introduced in Section IV. The stability analysis of nonlinear droop-controlled μG is discussed in the Section V. The performance of the proposed method is investigated through the case studies conducted in Section VI. In addition, simulation and experimental studies are presented in Section VII to verify the effectiveness of the nonlinear droop control in the μG operating cost minimization. Finally, the paper is concluded in Section VIII.

II. Droop Control Techniques

The droop control is one of the most widely used methods in the islanded μGs which regulates frequency and voltage to adjust the amount of the power flow among the DGs. The foundation of the droop concept can be understood from a simplified model of a DG connected to a μG through inductive lines, as shown in Fig. 2.

The voltage of the ith DG unit here can be expressed as $v_{\mathrm{DG}_i} = \sqrt{2}\, E_i \sin(\omega t + \delta_i)$. Assuming that the μG common-bus voltage as a reference voltage (V_o), the output active and reactive power (P_i and Q_i) of ith DG unit can be calculated as

$$P_i = \frac{E_i V_o \sin\delta_i}{X_{Li}} \qquad Q_i = \frac{V_o\,(E_i\cos\delta_i - V_o)}{X_{Li}} \tag{1}$$

where E_i is the magnitude of the ith DG unit voltage and X_{Li} is the coupling line impedance. Here, the phase difference between the ith DG unit and bus voltage (δ_i) are usually very small and accordingly, the assumptions of $\sin\delta_i \approx \delta_i$ and $\cos\delta_i \approx 1$ can be made. Based on these assumptions, it is clear that the produced active power is mainly dependent on δ_i, which can be easily manipulated by controlling the frequency of inverters. On the other hand, the reactive power generation is mainly dependent on the voltage difference ($E_i - V_o$), which can be controlled by adjusting E_i. Therefore, the frequency and voltage parameters of DGs are effectively used in droop control to regulate the amount of the power generation. In droop control, the frequency and voltage regulation are basically performed by applying a negative feedback in the frequency and the voltage of the DG according to the produced active and reactive power. In the literature, three different droop control methods have been proposed: linear, dynamic and nonlinear droop control [21]–[29] for different purposes.

Linear droop control (also known as conventional droop control) is typically implemented at each DG unit as a local controller in the primary control level (see Fig. 1) and designed to fulfill the following tasks [11], [30]–[35]:

1) frequency and voltage regulation in islanded μGs;
2) proportional power sharing among the DGs without the need of a communication link;
3) introducing plug-and-play capability for DGs;
4) mitigation of undesired circulating currents among the DGs.

Linear droop controller achieves these tasks by performing frequency and voltage regulations using the following relations:

$$f_{\mathrm{opt}} = \ f_i = f_{\mathrm{ref}} \ - k_{p,i} P_i \tag{2}$$

$$E_i = \ E_{\mathrm{ref}} \ - k_{q,i} Q_i \tag{3}$$

where f_i and E_i are the actual frequency and voltage of the i^{th} DG, respectively. The constant parameters f_{ref} and E_{ref} are the predefined reference frequency and voltage values, respectively, and the values $k_{p,i}$ and $k_{q,i}$ are the frequency and voltage droop coefficients. Since the frequency is a universal signal over the μG, frequencies of all DGs have the same value as the μG operating frequency (f_{opt}) at steady-state operation regardless of μG topology. Hence, the amount of the frequency droops of all DGs is equal to each other at steady-state operation, i.e., $k_{p,1}\ P_1 = k_{p,2}\ P_2 = \ \ldots\ = k_{p,N_s}\ P_{N_s}$. This fact allows the linear droop controller to perform a precise proportional active power sharing among the DGs by selecting the $k_{p,i}$ values based on the active power ratings of the DGs [11]. On the other hand, the voltage is not a universal signal, and so the linear droop controller may not lead to an accurate proportional reactive power sharing due to the presence of line impedances. The details of accurate proportional reactive power sharing will not be covered in this paper due to its negligible effect on cost-effective μG operation [22]. Interested readers can find more details in [11], [13], [18], [19], [34], and [37]. In the case of μG with low voltage, the coupling lines are mainly resistive. This resistive line could impose a strong coupling between real and reactive power. Although this paper focuses mainly on real power sharing as it is the main component that impacts the operating cost, methods such as [38]–[41] could be used to eliminate the impact of this coupling on the system dynamics response and stability. In a linear droop method, the $k_{p,i}$ value for each DG is calculated as

$$k_{p,i} = \ \Delta \mathrm{f}_{\max} / P_{i,\max} \tag{4}$$

where $P_{i,\max}$ is maximum available power of i^{th} DG, and $\Delta f_{\max}$ is the maximum acceptable frequency droop in the μG. The $\Delta f_{\max}$ value must be taken into consideration to limit the frequency deviation at $P_{i,\max}$ [39]. Fig. 3 illustrates the frequency variation and corresponding power sharing among two DGs rated differently. As seen from the droop curves, the positive load variation leads to a slight deviation in f_{opt}, and

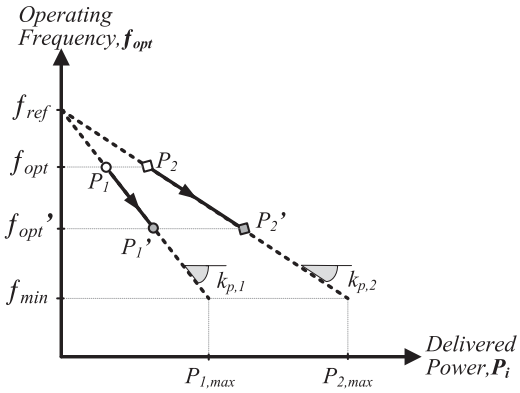

Fig. 3. Operating frequency variation in linear droop-controlled μGs.

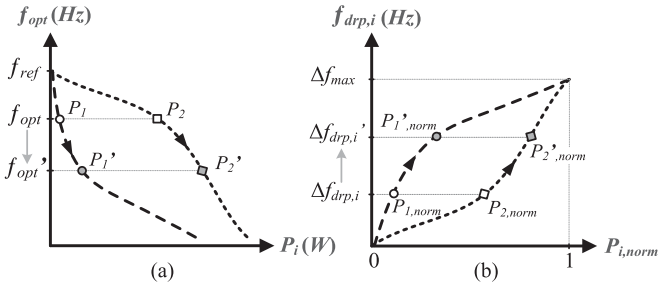

Fig. 4. (a) Operating frequency variation in nonlinear droop method and (b) nonlinear frequency droop versus normalized active power.

the frequencies of both DGs stabilize at a certain value $f_{\rm opt}{}'$. The projection of $f_{\rm opt}{}'$ value over the droop curves shows how the new load power is shared between the participating DGs. As seen, the real power generations of the DGs at any loading condition are always proportional to their power ratings in the linear droop control method. As mentioned earlier, the linear droop control is very simple, reliable, and flexible method; however, linear power sharing based on the power ratings may not be a cost-effective strategy to minimize the μG operating cost [21]–[29].

Dynamic droop control method has been introduced in [21] as an expansion of the linear droop control to reduce the total fuel cost of DGs in μGs. Unlike the linear droop control where the predefined reference frequency $f_{\rm ref}$ were static, the dynamic droop control utilizes $f_{\rm ref}$ as a dynamic signal in the control loop to regulate the active power produced by each DG in a way that the total amount of fuel consumption is reduced in the μG. In dynamic droop control, a centralized controller is utilized to determine the optimal power for each DG dynamically corresponding to instant load power. Then, the error between the instant power and the optimal power is passed through a PI controller to set the optimal $f_{\rm ref}$ value. Dynamic power sharing strategy introduces improved cost-effective μG operation compared the linear power sharing. However, it requires a centralized controller, whose single point-of-failure aspect degrades the network reliability. Moreover, the centralized controllers are costly due to the need of heavy connectivity in communication structures that covers the whole area of the μG [21], [36], [43]–[46]. Therefore, the idea of nonlinear droop control has been proposed in the literature as an alternative power sharing strategy to optimize the power sharing among DGs. The main advantage of the nonlinear droop control over the dynamic control is that the operation cost in the islanded μGs can be autonomously minimized without the need of a centralized controller. Nonlinear droop controller performs the optimal power sharing among the DGs by regulating the frequency as follows:

$$f_{\rm opt} = f_{\rm ref} \ - f_{{\rm drp},i}\left(.\right). \tag{5}$$

Here $f_{{\rm drp},i}(.)$ is the frequency droop relation changing as a function of the active output power of $\rm th$ DG, i.e., $f_{{\rm drp},i}(P_i) = \Delta f_{{\rm drp},1} = \Delta f_{{\rm drp},i}\ |_{i\,=\,2,3,\ldots,N_s}$, where N_s denotes the number of the DGs in the μG network. As illustrated in Fig. 4(a), the power demand is shared nonlinearly among the two nonlinear droop-controlled DGs based on their predefined $f_{{\rm drp},i}$. Fig. 4(b) shows the variation in both $f_{{\rm drp},i}$ and produced active power subsequent to a positive load change. As seen, the total frequency droop variation $\Delta f_{{\rm drp},i}$ of each DG are similar at steady-state operation. In contrast to the linear droop controller where the droop relations are simply constructed by a constant frequency droop coefficient selected based on only the power ratings, here the optimal $f_{{\rm drp},i}$ are required to be constructed in a way that minimizes the μG operating cost for all possible loading conditions.

As discussed in [26] and [27], while constructing the optimal $f_{{\rm drp},i}$ for each DG, it must always satisfy the following characteristics:

1) It should be a monotonic function satisfying the following property: $f_{{\rm drp},i}\left(P_i\right) < f_{{\rm drp},i}\left(P_i + \Delta P_i\right)$, for $P_i, \Delta P_i > 0$. This is required to obtain a single droop value for every loading condition and to provide a negative feedback in the droop relations. That is needed for stability purposes.
2) It should have a high degree of nonlinearity to improve the flexibility in constructing nonlinear droop relations.

The CFB method proposed in [23] and [24] constructs the $f_{{\rm drp},i}$ using the following expression:

$$f_{{\rm drp},i} = \ m_i C_{i,{\rm opt}}\left(P_i\right) \tag{6}$$

where $C_{i,{\rm opt}}$ is operating cost function of $i{\rm th}$ DG and m_i is the scaling factor that is calculated as $m_i = \Delta f_{\max}\ / C_{\max}$ to limit the frequency variation at $m_i = \Delta f_{\max}\ / C_{\max}$. The parameter $C_{\max}$ is the highest operating cost value among all DGs at their rated power and expressed as $C_{\max} = \max\left\{C_{i,{\rm opt}}(P_{i,\max})\right\}|_{i\,=\,1,2,\ldots,N_s}$. Constructing the droop relations $f_{\rm drp}$ only based on operating cost functions limit the flexibility and, accordingly, the cost effectiveness of the nonlinear droop controller. As an alternative approach, the NFB method defines the $f_{{\rm drp},i}$ as the combination of power functions whose exponents are considered positive integers and/or positive fractions as shown

$$f_{{\rm drp},i}(P_{i,{\rm norm}}) \ = \sum_{m=1}^{N}\left(K_{{\rm hi},m}\,P_{i,{\rm norm}}^{m} + K_{{\rm li},m}\,P_{i,{\rm norm}}^{1/(m+1)}\right) \tag{7}$$

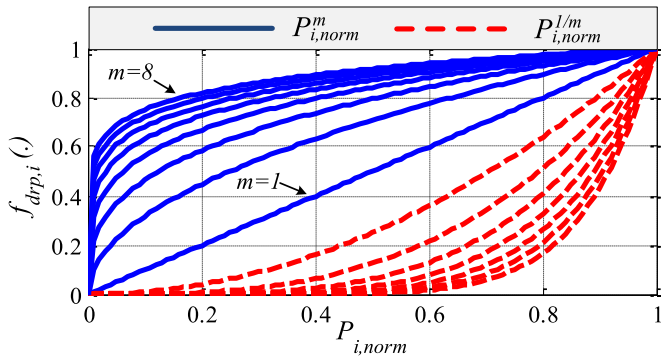

Fig. 5. Components of $f_{\mathrm{drp},i}$ at different degrees.

where $P_{i,\mathrm{norm}}$ is the normalized output power of the ith DG calculated as $P_{i,\mathrm{norm}} = P_i\ /P_{i,\mathrm{rated}}$ and N is the degree of the $f_{\mathrm{drp},i}$ function. This approach introduces more flexibility in constructing the optimal nonlinear droop relations compared to the CFB method and, consequently, improves the effectiveness of the nonlinear droop controller. However, the difficulty in NFB method is the proper selection of the coefficients $K_{\mathrm{hi},m}$ and $K_{\mathrm{li},m}$ so that the optimal nonlinear droop relations minimizing the μG operating cost can be constructed. The coefficients of power functions defined in (7) are constrained to be positive numbers so that the μG stability condition of $\partial f_{i,\mathrm{drp}}/\partial P_i > 0$ is always fulfilled for any constructed $f_{\mathrm{drp},i}$. Fig. 5 shows some possible waveforms that can be achieved using the $P^{m}_{i,\mathrm{norm}}$ and $P^{1/(m+1)}_{i,\mathrm{norm}}$ with different exponents. Clearly, various nonlinear droop relations can be constructed by combining these integer and fractional power functions with proper $K_{\mathrm{hi},m}$ and $K_{\mathrm{li},m}$ coefficient values. Adjusting the coefficients $K_{\mathrm{hi},m}$ and $K_{\mathrm{li},m}$ based on this formulation, provides more flexibility in shaping the $f_{\mathrm{drp},i}$ according to the desired droop behavior. Consequently, one can construct the optimal $f_{\mathrm{drp},i}$ for each $\mathrm{DG_i}$ with the proper selection of these coefficients and realize more cost-effective μG operation by implementing constructed $f_{\mathrm{drp},i}$ with a nonlinear droop controller.

As stated in previous section, the $K_{\mathrm{hi},m}$ and $K_{\mathrm{li},m+1}$ parameters for $m = 1,2,\ldots,N$ and $i = 1,2,\ldots,N_s$ have to be selected properly in order to achieve a cost-effective μG operation. Therefore, in [23], the NFB method specifies these parameters by solving the following optimization problem: select the values of $\{K_{\mathrm{hi},m},\ K_{\mathrm{li},m+1}\}\ |_{m\ =\ 1,2,\ldots,N,\ i\ =\ 1,2,\ldots,N_s}$ that minimize the μG total cost function $C_{\mu\mathrm{G}}(.)$, which is expressed as

$$C_{\mu G} = \sum_{j=1}^{k}\sum_{i=1}^{N_s} C_{i,\mathrm{opt}}\left(P_{i,j}\right)$$

$$\text{subject to}\ \begin{cases} P_{i,\min} \le P_{i,j} \le P_{i,\max} \\ P_{\mathrm{Load},j} = \sum_{i=1}^{N_s} P_{i,j} \\ \Delta f_{\mathrm{drp},1} = \Delta f_{\mathrm{drp},i}|_{i=2,3,\ldots,N_s} \end{cases} \tag{8}$$

where $C_{i,\mathrm{opt}}$ is the operating cost function of the ith DG (DG_i), and $P_{i,j}$ is the produced power by DG_i at the jth loading condition. The parameters N_s and k represent the total number of DGs in the μG network and the considered number of loading conditions, respectively, and $P_{\mathrm{Load},j}$ is the power demand at the jth loading condition. The value of k is selected to ensure that a representative set of loading conditions is considered such that the optimized parameters should minimize the operation cost under all loading conditions. After solving the optimization problem defined in (8), the resulting $\{K_{\mathrm{hi},m},\ K_{\mathrm{li},m+1}\}\ |_{m\ =\ 1,2,\ldots,N,\ i\ =\ 1,2,\ldots,N_s}$ values are used in (7) to define the optimal droop relations for each participating DG.

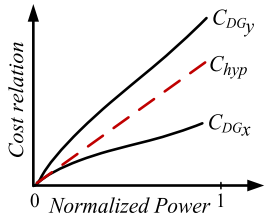

Fig. 6. Operating cost relations considered for xth and yth DGs.

The NFB method reduces the μG operating cost compared to conventional droop relations. However, the optimization scheme used in the NFB method is μG topology-dependent due to the necessity of redefining the entire optimization algorithm after any modification in the topology such as elimination or addition of a DG. Accordingly, it does not support the plug-and-play capability required for the μG operation. The main motivation of this paper is thus to introduce a new optimization scheme that supports the nonlinear droop control with the plug and play capability in addition to investigate the possibility of enhancing the performance of the NFB method.

III. Plug-and-Play Optimization Scheme

The optimal nonlinear frequency droop relation for each DG need to be constructed independently to achieve a μG topology-independent cost optimization. In this paper, a PPOS is proposed to enable the nonlinear droop control method to inherit the following salient features:

1) the frequency and voltage regulation in the islanded μGs;
2) cost-effective operation in islanded μGs without the need of a communication link;
3) plug-and-play facility for the DGs.

The main target of this paper is to construct optimal nonlinear droop relation for each participating DG independently. To achieve that, each DG can be optimized with a hypothetical reference DG. In order to construct an indirect optimization platform for droop relations of all DGs, the cost curve and droop relation of this reference DG needs to be predefined. Suppose that the cost curve of xth (C_{DG_x}) and yth (C_{DG_x}) DGs in a μG and the cost curve of the hypothetical DG (C_{hyp}) are as shown in Fig. 6. As seen, the operating cost of xth DG is always lower than the operating cost of the hypothetical DG, which is vice versa for yth DG. Clearly, an economical power sharing among

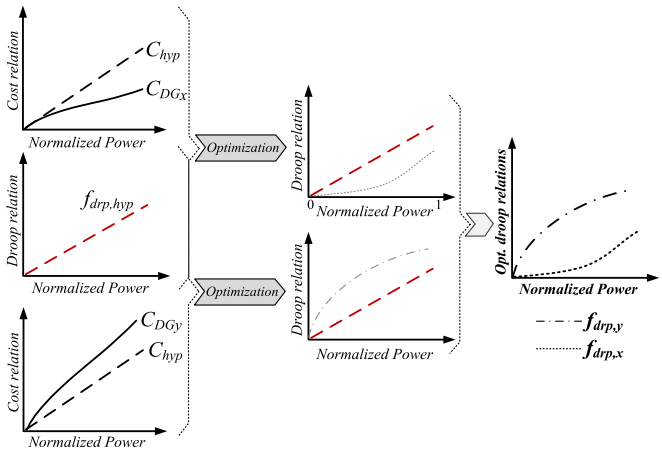

Fig. 7. Overall droop relation construction process.

xth and yth DGs can be realized by selecting any droop relation for xth DG lower than the droop relation of th DG.

To find out the optimal droop relation for xth DG independently from the yth DG, the droop relation of the hypothetical DG can be defined as a global reference droop relation. Then, an optimization scheme can be developed based on this reference droop relation and used to seek only the droop relation for xth DG (or th xDG) that introduces optimal power sharing between the xth DG (or yth DG) and the hypothetical DG. In that regard, this optimization scheme needs to be designed properly such that the droop relation of every DG is positioned at its optimal place around the reference droop relation according to their operating cost curves.

Fig. 7 illustrates the overall process of droop relation construction for each DG in which the droop relation of the hypothetical DG ($f_{\mathrm{drp,hyp}}$) is predefined and used during the optimization. Here, the optimization scheme needs to be designed properly such that it can seek optimal coefficients $\{K_{\mathrm{hx},m},\ K_{\mathrm{lx},m+1}\}\,|_{m\,=\,1,2,\ldots,N}$ in (7) to find out the optimal placement for the droop relation of th DG, $f_{\mathrm{drp},x}$. Due to the cost relations shown in Fig. 7, the optimization scheme is expected to place $f_{\mathrm{drp},x}$ in a region under the $f_{\mathrm{drp,hyp}}$ so that an economical power sharing between the xth DG and hypothetical DG can be realized. When the similar optimization is computed for the th DG, its optimal droop relation $f_{\mathrm{drp},y}$ is expected to be placed in the region above $f_{\mathrm{drp,hyp}}$ since its operating cost is always higher than hypothetical DG. In that particular case, the prospective optimal droop relations for xth and yth DGs is shown in Fig. 7. With these resulting droop relations, an economical power sharing among xth and yth DGs can be achieved although their droop relations are optimized independently. However, several computations have shown that the optimization scheme designed with single hypothetical DG does not guarantee resulting proper droop relations. As an example, since C_{DG_x} is always lower than C_{hyp} at any operating point (see Fig. 6), improved economical power sharing can be realized as more power is derived from the th DG. Therefore, the optimization scheme will force $f_{\mathrm{drp},x}$ to be far down from $f_{\mathrm{drp,hyp}}$ during the optimization process to reach optimal power sharing among the xth DG and the hypothetical DG. In case of y_{th} DG, its droop relation will be forced to place far up from the $\mathrm{f}_{\mathrm{drp,hyp}}$ due to its high operating cost. Suppose that there is another DG whose operating cost curve is between C_{DG_x} and C_{hyp}. Since its cost curve is lower than C_{hyp}, its droop relation will also be forced to place far down from $f_{\mathrm{drp,hyp}}$. At the end of the optimization, its droop relation may end up being similar with the droop relation of th DG, which is not desired since their operating cost curves are different. Therefore, this paper proposes an optimization scheme that is designed with two hypothetical reference DGs in order to avoid the aforementioned issue.

The proposed scheme is designed to perform an optimization for each DG against two user-defined hypothetical reference DGs ($\mathrm{DG_{hyp}}$). It consists of an optimization problem that is defined based on the $\mathrm{DG_{hyp}}$s and the DG_i whose optimal nonlinear droop relation is aimed to be constructed. As a first step to overcome the aforementioned issue, the cost relations of these reference DGs are predefined in such a way that they form an envelope for possible cost relations of DGs in a μG. For that purpose, the operating cost relations of these reference DGs (C_{hyp_1} and C_{hyp_2}) are expressed as follows:

$$C_{\mathrm{hyp}_q} \;=\; c_{\mathrm{hyp}_q}\ P_{\mathrm{norm}} \tag{9}$$

$$c_{\mathrm{hyp}_1} \;<\; \{C_{i,\mathrm{opt}}\,(P_{i,\mathrm{max}})\ |_{i\,=\,1,2,\ldots,N_s}\} < c_{\mathrm{hyp}_2} \tag{10}$$

where c_{hyp_1} and c_{hyp_2} are the cost coefficients that are selected systematically to be, respectively, lower and higher than the maximum operating cost of all DGs as shown in (10). Thus, the coefficients c_{hyp_1} and c_{hyp_2} can be defined as

$$c_{\mathrm{hyp}_1} \;=\; \min\{C_{i,\mathrm{opt}}\,(P_{i,\mathrm{max}})\ |_{i\,=\,1,2,\ldots,N_s}\} \times \frac{1}{\alpha} \tag{11}$$

$$c_{\mathrm{hyp}_2} \;=\; \max\{C_{i,\mathrm{opt}}\,(P_{i,\mathrm{max}})\ |_{i\,=\,1,2,\ldots,N_s}\} \times \alpha \tag{12}$$

where α represents a constant value,which can be selected properly in the range of [1.0, 2.0] to form a satisfactory envelope for all possible cost relations. Clearly, different α values result in different set of cost coefficients and accordingly,it may affect the performance of the proposed optimization scheme.However,these cost coefficients are predefined once and used as global parameters while performing optimization for each DG against two hypothetical reference DGs.Therefore,they will have similar effect while constructing optimal nonlinear droop relation for each DG independently. As the second step,the droop relations of the reference DGs are predefined such that it limits the possible droop relations and,accordingly, assist the optimization scheme seek proper droop relations during the optimization process.Here,the droop relations ($f_{\mathrm{drp,hyp}_1}$ and $f_{\mathrm{drp,hyp}_2}$) of the hypothetical DGs are defined based on the selected c_{hyp_1} and c_{hyp_2} values using the following expressions:

$$f_{\mathrm{drp,hyp_q}} \;=\; k_{\mathrm{ref}_q}\ P_{\mathrm{norm}} \tag{13}$$

$$k_{\mathrm{ref}_q} \;=\; m\ c_{\mathrm{hyp}_q}/P_{\mathrm{hyp}_q,\mathrm{max}} \tag{14}$$

where k_{ref_q} and m are the reference droop coefficient and the conversion factor, respectively, and $P_{\mathrm{hyp}_q,\mathrm{max}}$ is the maximum power of $\mathrm{DG_{hyp}}_q$, which is considered to be identical with the maximum power of the DG_i. It must be noticed that all the cost

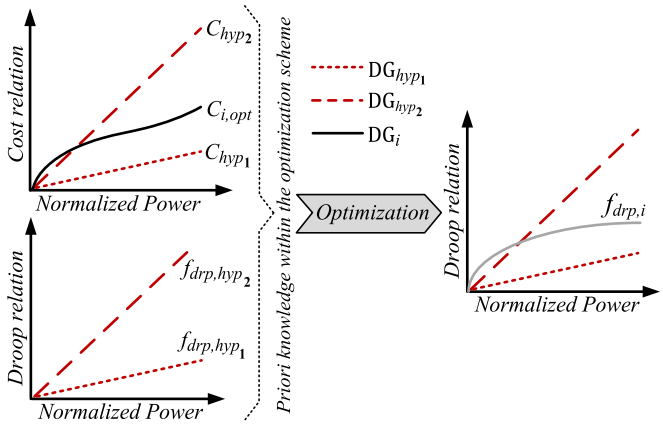

Fig. 8. Operating cost and droop relations defined for the hypothetical DGs.

and the droop relations evaluated in the PPOS are formulated as a function of normalized power P_{norm}.

Fig. 8 illustrates the configuration of the operating cost and droop relations designed for the hypothetical DGs. Assuming a DG_i whose operating cost relation is as shown in Fig. 8, the optimal power sharing among the DG_i and the DG_{hyp}s can be only realized by placing the $f_{\text{drp},i}$ somewhere between the droop relations of the DG_{hyp}s. Thus, this configuration basically provides both upper and lower boundaries to the PPOS to avoid constructing relatively very high or low nonlinear droop relations while searching the optimal placement for the $f_{\text{drp},i}$. Clearly, the optimal placement for the $f_{\text{drp},i}$ is directly associated with the operating cost relation of DG_i. The developed optimization scheme performs an offline optimization process for each DG individually with respect to two hypothetical DGs. This way of construction makes the optimization method proposed in this paper independent from the μG topology and so named as PPOS. This feature eliminates the main limitation of the NFB method and enables the nonlinear droop control to maintain the plug-and-play facility for the DGs while introducing cost-effective μG operation.

A. Formulation of Optimization Problem

In the stage of constructing the optimal $f_{\text{drp},i}$, the set of the coefficients $\{K_{\text{hi},m},\ K_{\text{li},m+1}\}\,|_{m\,=\,1,2,\ldots,N}$ in (7) have to be properly selected to realize optimal power sharing among the DG_i and the DG_{hyp}s. Accordingly, the optimization problem can be defined as following: select the values of $\{K_{\text{hi},m},\ K_{\text{li},m+1}\}\,|_{m\,=\,1,2,\ldots,N}$ that minimize the $C_{\text{total}}(.)$ formulated as

$$C_{\text{total}} = \sum_{j=1}^{k}\left\{C_{i,\text{opt}}\left(P_{i,j}\right) + C_{\text{hyp}_1}\left(P_{\text{hyp}_1,j}\right) + C_{\text{hyp}_2}\left(P_{\text{hyp}_2,j}\right)\right\}$$

$$\text{subject to}\begin{cases} P_{i,\min} \le \left\{P_{i,j}\ ,\ P_{\text{hyp}_1,j}\ ,\ P_{\text{hyp}_2,j}\right\} \le P_{i,\max} \\ P_{\text{Load},j} = P_{i,j} + P_{\text{hyp}_1,j} + P_{\text{hyp}_2,j} \\ f_{\text{drp},i}\left(P_{i,j}\right) = f_{\text{drp,hyp}_q}\left(P_{\text{hyp}_q,j}\right)\,|_{q=1,2} \end{cases} \tag{15}$$

where the parameters $P_{i,j}$, $P_{\text{hyp}_1,j}$, and $P_{\text{hyp}_2,j}$ are the output power of the DG_i, DG_{hyp_1}, and DG_{hyp_2} at the jth loading condition ($P_{\text{Load},j}$), respectively. The value of k in the summation operator is the representative set of loading condition which is obtained by increasing the load value from the smallest value ($P_{\text{Load},1}$) to the highest value ($P_{\text{Load},k}$) with fixed steps, where the maximum power demand calculated as $P_{\text{Load,max}} = P_{i,\max} + P_{\text{hyp}_1,\max} + P_{\text{hyp}_2,\max}$. Here, the droop and cost relations of the DG_{hyp}s are predefined using (9) and (11)–(14), and so the power sharing among the DG_i, DG_{hyp_1}, and DG_{hyp_2} is mainly dictated by the $f_{\text{drp},i}$, which can be easily determined after setting the values of $\{K_{\text{hi},m},\ K_{\text{li},m+1}\}\,|_{m\,=\,1,2,\ldots,N}$. Thus, one needs to first select a set of coefficient values as a first step in calculating the C_{total}. Based on these selected coefficients values, the output power values of DG_i, DG_{hyp_1}, and DG_{hyp_2} need to be calculated subject to the constraints defined in (15), and accordingly, the corresponding operating cost values $C_{DG_i}(P_{i,j})$, $C_{\text{hyp}_1}(P_{\text{hyp}_1,j})$, and $C_{\text{hyp}_1}(P_{\text{hyp}_2,j})$ can be calculated to determine the total cost at $P_{\text{Load},j}$. For the same selected set of coefficients values, this procedure is required to be repeated at each loading step to calculate the C_{total}. However, the optimal set of coefficients $\{K^{\text{opt}}_{\text{hi},m},\ K^{\text{opt}}_{\text{li},m+1}\}|_{m\,=\,1,2,\ldots,N}$, resulting the minimum C_{total} value have to be searched to solve the optimization problem defined in (15). Due to the complexity and difficulty of solving this optimization problem, heuristic optimization tools (e.g., particle swarm, evolutionary computation, ant colony, artificial beer colony, and tabu search) can be utilized effectively to achieve fast convergence to the satisfactory solutions [47]. Among the heuristic optimization techniques, particle swarm optimization (PSO) has been found to be a suitable and an effective technique for the optimization problem in this study.

The PSO is a stochastic computation technique originally adapted from the collective food searching behavior of animals such as birds flocking and fish schooling [48]. This optimization technique provides a population-based exploration process in which particles collectively search for the optimum. Here, each particle actually means a real number set that corresponds to a potential solution in a search space. As an initial process in the PSO, a number of particles are randomly generated. Then, each particle updates its velocity and position iteratively based on the past experience to reach optimal position that converges the global best solution for the optimization problem. In a basic PSO algorithm, each particle has both velocity and position vectors that are adjusted at each search iteration according to the following formulas:

$$\begin{aligned}\mathbf{v}_n^{k+1} &= \omega^k \mathbf{v}_n^k + \alpha_1 r_1\left[\mathbf{x}_{p\text{best},n} - \mathbf{x}_n^{k+1}\right] \\ &\quad + \alpha_2 r_2\left[\mathbf{x}_{g\text{best}} - \mathbf{x}_n^{k+1}\right]\end{aligned} \tag{16}$$

$$\mathbf{x}_n^{k+1} = \mathbf{x}_n^k + \mathbf{v}_n^{k+1} \tag{17}$$

where vectors $\mathbf{v}_n^k = [v_{n_1}, v_{n_2}, \ldots, v_{n_q}]^{\text{T}}$ and $\mathbf{x}_n^k = [x_{n_1}, x_{n_2}, \ldots, x_{n_q}]^{\text{T}}$ represent the velocity and position of the nth particle at kth iteration in the q-dimensional search space, respectively. Besides, vector $\mathbf{x}_{\text{pbest},n} = [x_{\text{pbest},n_1}, x_{\text{pbest},n_1}, \ldots, x_{\text{pbest},n_q}]^{\text{T}}$ denotes the personal position which

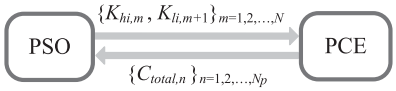

Fig. 9. Block diagram of the stages in the PPOS.

corresponds to the best personal fitness value, $f(\mathbf{x}_{\mathrm{pbest},n})$, recorded for the nth particle. Similarly, vector $\mathbf{x}_{\mathrm{gbest}} = [x_{\mathrm{gbest}_1}, x_{\mathrm{gbest}_2}, \ldots, x_{\mathrm{gbest}_q}]^{\mathrm{T}}$ denotes the global best position visited by any particle in the population and corresponds to the best global fitness value $f(\mathbf{x}\_\mathrm{gbest}, n)$, recorded up to recent iteration.

B. Implementation of PSO

In this paper, a PSO algorithm is implemented to solve the optimization problem defined in (15). Here, the PSO technique is mainly employed to search the optimal set of the coefficients, $\{K_{\mathrm{hi},m}^{\mathrm{opt}},\ K_{\mathrm{li},m+1}^{\mathrm{opt}}\}|_{m\,=\,1,2,\ldots,N}$, which is later used in (7) to define the optimal nonlinear droop relation for the DG_i. The optimal droop relations constructed by the PPOS for each DG are implemented in the nonlinear droop controller to perform economical power sharing among the N_s number of DGs at any loading condition and consequently, the total μG operating cost can be effectively minimized.

In the PSO algorithm developed in this paper, the population consists of N_p particles, i.e., $n = 1, 2, \ldots, N_p$, and each particle is defined as vector $\mathbf{x}_n = [K_{\mathrm{hi},1}, \ldots, K_{\mathrm{hi},N}, K_{\mathrm{li},2}, \ldots, K_{\mathrm{li},N}]^{\mathrm{T}}$. To update the particles' positions using (16) and (17), the vectors $\mathbf{x}_{\mathrm{pbest},n}$ and $\mathbf{x}_{\mathrm{gbest},n}$ need be determined according to the personal best fitness value of each particle and the global best fitness value up to the recent iteration. The fitness value associated with each particle can be determined from the defined fitness function and the constraints can be easily satisfied by keeping the position of the particles in the range [0,4] during the iteration process. However, calculating the fitness value associated with each particle in (15) is complicated due to the indirect relation between the elements of the vector $\mathbf{x}$ and the fitness function C_{total}. Thus, this optimization problem requires another stage, which is denoted here as power and cost evaluation (PCE). The block diagram of the stages developed for the PPOS is shown in Fig. 9.

In the stage of PCE, the power sharing among the DG_i, $\mathrm{DG}_{\mathrm{hyp}_1}$, and $\mathrm{DG}_{\mathrm{hyp}_2}$ is first calculated based on the selected particle at a certain loading condition. This calculation is repeated for all possible loading conditions while checking the constraints defined in (15) in order to determine the C_{total} for the selected particle. The PCE stage determines the C_{total} for all particles in the population and then proceeds a vector whose elements denotes the fitness value of each particle, i.e.,$\mathbf{C} = [C_{\mathrm{total},1}, C_{\mathrm{total},2}\ \ldots, C_{\mathrm{total},N_p}]^{\mathrm{T}}$, to the PSO stage. In PSO stage, the vectors $\mathbf{x}_{\mathrm{pbest},n}$ and $\mathbf{x}_{\mathrm{gbest},n}$ are first evaluated and then the particles' positions are updated using (16) and (17). These updated particles are again sent to the PCE stage to evaluate the fitness values of the updated particles. This process between these two stages is repeated iteratively until the PPOS finds the optimal set of $\{K_{\mathrm{hi},m}^{\mathrm{opt}},\ K_{\mathrm{li},m+1}^{\mathrm{opt}}\}|_{m\,=\,1,2,\ldots,N}$ for the DG_i. If one considers a μG that consists of N_s number of DGs, the PPOS needs to be proceeded N_s times to construct optimal nonlinear droop relations for every DG individually. It must be noted that after any selection for the droop parameters is made, the stability condition is checked within the PPOS using the stability checking method discussed in the following section. Accordingly, any droop relation (or particle) leading to instability is eliminated and not evaluated during the optimization process to assist the PPSO converge only stable droop relations. Once all the droop relations constructed, the stability can be rechecked to verify using the stability checking method, which will be discussed in detail in the following section.

IV. Stability Analysis of Nonlinear Droop-Controlled Microgrids

In this section, a mathematical tool is developed to analyze the stability of a μG with DGs derived by the PPOS-based droop controllers. As investigated in [27], dominant low-frequency modes are principally dictated by power dynamics. Hence, the stable operation of a μG can be ensured by simply analyzing the dynamics of the power sharing which consists of droop controller and low-pass filter. In a typical power sharing mechanism of a μG that combines N_s number of DGs, first, the instantaneous power measurements p_i and q_i are passed through low-pass filters as follows:

$$P_i = \frac{\omega_c}{s+\omega_c}\, p_i \tag{18}$$

$$Q_i = \frac{\omega_c}{s+\omega_c}\, q_i \tag{19}$$

where P_i and Q_i are filtered versions of real and reactive power components of the ith DG, respectively, which are used in the droop relations defined in (3) and (5). Here, the parameter ω_c is the filter cutoff frequency. Accordingly, the expressions in (18) and (19) can be represented in time domain as

$$\dot{P}_i = \omega_c\ (p_i - P_i) \tag{20}$$

$$\dot{Q}_i = \omega_c\ (q_i - Q_i) \tag{21}$$

where dots above the variables denotes the derivation with respect to time. In nonlinear frequency droop-controlled μGs, the phase of the ith DG θ_i is given as

$$\theta_i = 2\pi \int (f_{\mathrm{ref}} - f_{\mathrm{drp},i}) \tag{22}$$

where f_{ref} is a constant value that is utilized for all DGs. As discussed in [27], the phase of one of the DGs can be considered as a reference and accordingly, the phase difference can be calculated as

$$\dot{\delta}_i = \dot{\theta}_i - \dot{\theta}_{\mathrm{ref}} = 2\pi\ (f_{\mathrm{drp,ref}} - f_{\mathrm{drp},i}) \tag{23}$$

where δ_i is the phase difference between the ith DG and the reference source $\mathrm{DG}_{\mathrm{ref}}$. Equations (20), (21), and (23) describe the dynamics of a DG with the nonlinear frequency droop controller. To obtain small-signal model, these nonlinear equations

need to be linearized as follows:

$$\dot{\tilde{P}}_i = \omega_c \left(\tilde{p}_i - \tilde{P}_i\right) \tag{24}$$

$$\dot{\tilde{Q}}_i = \omega_c \left(\tilde{q}_i - \tilde{Q}_i\right) \tag{25}$$

$$\dot{\tilde{\delta}}_i = 2\pi \left[\left(\frac{\partial f_{\mathrm{drp,ref}}}{\partial P_{\mathrm{ref}}}\bigg|_{P_{\mathrm{ref}}=\hat{P}_{\mathrm{ref}}} \right) \tilde{P}_{\mathrm{ref}} - \left(\frac{\partial f_{\mathrm{drp},i}}{\partial P_i}\bigg|_{P_i=\hat{P}_i} \right) \tilde{P}_i \right] \tag{26}$$

where the symbols $\sim$ and $\wedge$ represent the perturbed variables and equilibrium point values. Equations (24)–(26) can be given in a standard form as

$$\dot{\tilde{\mathbf{x}}} = \mathbf{G}\tilde{\mathbf{x}} + \mathrm{H}\tilde{\mathbf{w}} \tag{27}$$

$$\tilde{\mathbf{x}} = \left[\, \tilde{P}_1 \ \tilde{Q}_1 \ \tilde{\delta}_1 \ \cdots \ \tilde{P}_{\mathrm{ref}} \ \tilde{Q}_{\mathrm{ref}} \ \cdots \tilde{P}_{N_s} \ \tilde{Q}_{N_s} \ \tilde{\delta}_{N_s} \,\right]^{\mathrm{T}} \tag{28}$$

$$\tilde{\mathbf{w}} = \left[\tilde{p}_1 \quad \tilde{q}_1 \quad \cdots \quad \tilde{p}_{N_s} \quad \tilde{q}_{N_s}\right]^{\mathrm{T}} \tag{29}$$

where $\mathbf{G}$ and H are state and auxiliary matrices, respectively, and $\tilde{\mathbf{x}} \in {}^{(3N_s-1)\times 1}$ and $\tilde{\mathbf{w}} \in {}^{2N_s\times 1}$ are the vectors of states and auxiliary variables, respectively. The values of auxiliary variables can be obtained through load flow analysis (LFA) in which the set of relations $\mathbf{\Psi}$ is given as

$$\mathbf{\Psi}\left(\cdots, E_i, \delta_i, \ p_i, q_i, \cdots\right) = 0. \tag{30}$$

By using the (3), $\mathbf{\Psi}$ can be described in terms of the states and auxiliary variables only $\mathbf{\Psi}'$ as follows:

$$\mathbf{\Psi}'\left(\cdots, Q_i, \delta_i, \ p_i, q_i, \cdots\right) = 0. \tag{31}$$

The linearization of $\mathbf{\Psi}$ can be performed as

$$\left(\frac{\partial \mathbf{\Psi}}{\partial \mathbf{x}}\bigg|_{\substack{\mathrm{x}=\hat{\mathbf{x}} \\ \mathrm{w}=\hat{\mathbf{w}}}} \right) \tilde{\mathbf{x}} + \left(\frac{\partial \mathbf{\Psi}}{\partial \mathbf{w}}\bigg|_{\substack{\mathrm{x}=\hat{\mathbf{x}} \\ \mathrm{w}=\hat{\mathbf{w}}}} \right) \tilde{\mathbf{w}} = 0. \tag{32}$$

Finally, (32) can be modified in terms of $\tilde{\mathbf{w}}$ and then substituted into (27) to obtain the linearized μG model as

$$\dot{\tilde{\mathbf{x}}} = \mathbf{G}\tilde{\mathbf{x}} - \mathrm{H}\left(\frac{\partial \mathbf{\Psi}}{\partial \mathbf{w}}\bigg|_{\substack{\mathrm{x}=\hat{\mathbf{x}} \\ \mathrm{w}=\hat{\mathbf{w}}}} \right)^{-1} \left(\frac{\partial \mathbf{\Psi}}{\partial \mathbf{x}}\bigg|_{\substack{\mathrm{x}=\hat{\mathbf{x}} \\ \mathrm{w}=\hat{\mathbf{w}}}} \right) \tilde{\mathbf{x}} = \mathbf{A}\tilde{\mathbf{x}} \tag{33}$$

where $\mathbf{A}$ is known as the system matrix. One can easily check the stability of the μG system by observing the eigenvalues of the matrix $\mathbf{A}$, which are required to be negative under all loading conditions for stable μG operation. Since the matrix $\mathbf{A}$ is subject to changes due to the load variations in the μG system, the trajectory of the eigenvalues of the matrix $\mathbf{A}$ under normal and highly stressing loadings need to be observed to guarantee stable operation for all loading conditions. The eigenvalues of the matrix $\mathbf{A}$ in (33) show whether the μG is stable or not. However, this conclusion is true for just a single operating point. In reality, there are number of nonlinearities in the original model of the μG before linearization including the sine and cosine of the angle δ, the voltage and current product to obtain the power in addition to the proposed nonlinear droop relations. To ensure the stability of the μG under all loading conditions, after every iteration for solving the optimization problem explained in Section II-B, the matrix $\mathbf{A}$ is obtained and its eigenvalues are evaluated. If at least one of these eigenvalues is found to be unstable, the droop parameters of sources will be multiplied by a factor and the process repeats. These calculations continue till the selected set of droop parameters satisfy the stability conditions under all loading conditions. It is important to indicate that the stability of the individual operating points might not necessarily ensure the stability of the whole system. This is a well-known fact in the field stability of switches systems that switches between various modes of operation [49]. However, as indicated in [50], the stability of a system that switches between a number of stable modes could be ensured if it stays in the new mode for a period of time sufficient for its dynamics to settle to the steady state. Clearly, the load variations in power systems are much slower than the current and voltage dynamics in the line which satisfies the condition indicated in [50].

V. Case Study

As stated in [28] and [29], the CFB method is an improved method compared to the method introduced in [22] and it develops nonlinear droop relations for each DG based on their operating cost functions in order to realize economical power sharing. On the other hand, the MCB method introduces much simpler solution by developing linear droop relations based on maximum or mean operating costs of DGs. These methods have been further improved in [28] and [29] where the droop relations are designed such that the costlier DGs are autonomously turned off during the light loadings and operated only during high loadings, which provide considerable cost savings particularly when no loading operating costs are taken into account. As an alternative method, the NFB has been also used to reduce the μG operation cost; however, it incapacitates the plug-and-play capability required for the μG operation. In this paper, similar to the CFB and MCB methods, the PPOS has been developed to construct the optimal nonlinear droop relations with maintained the plug-and-play capability to realize an economical power sharing considering that all DGs are preferred to be operated continuously at all loading conditions. Thus, the case study in this section compares the cost-saving performance of the PPOS with only the CFB and the MCB methods.

In this section, a set of realistic cost curves have been used to demonstrate the effectiveness of the PPOS on minimizing the μG operation cost. The cost-saving advantage of the PPOS over the proposed methods has been verified by exploring the percentage operating cost savings of the nonlinear droop relations with respect to the conventional droop relation. The μG system considered in this case study consists of three DGs equivalently rated at 2 kW and their operating cost curves are shown in Fig. 10. These operating cost curves have been analyzed previously in [25] as real generation cost data for different type of DGs to test the performance of the MCB method.

The optimization problem has been solved for the considered μG to construct the optimal nonlinear droop relations for all

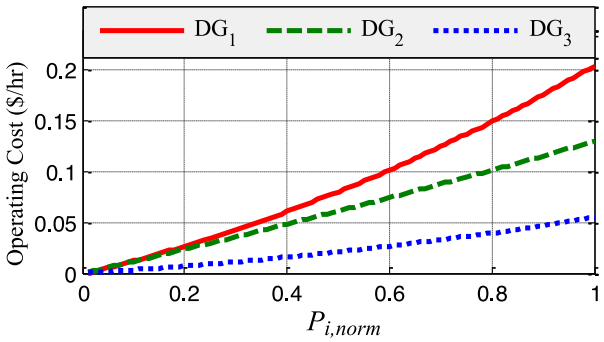

Fig. 10. Real operating cost curves analyzed in [25].

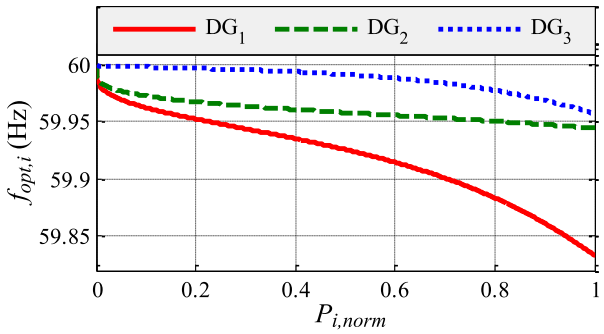

Fig. 11. Nonlinear droop relations obtained using the PPOS.

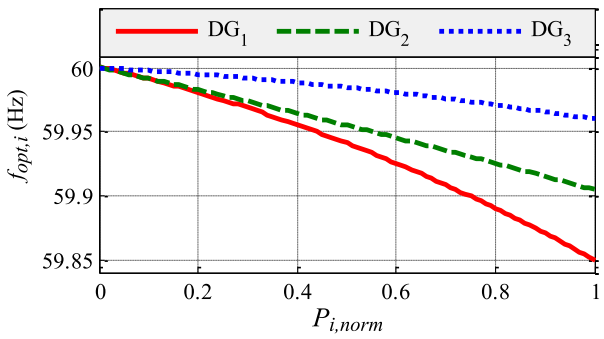

Fig. 12. Nonlinear droop relations obtained using the CFB method.

DGs. After selecting the value of α in (11) and (12) as 2.0, the cost coefficients c_{hyp_1} and c_{hyp_2} for the hypothetical DGs have been found as 0.027 and 0.4, respectively. These coefficient values have been used in (10) to form proper cost relations for the hypothetical DGs. To provide also a proper boundary for the optimal droop relation of DG_i while being constructed by the PPOS, the droop relations of the hypothetical DGs have been defined using (14) with the conversion factor of 1.0. The optimal selection of $\{K_{\mathrm{hi},m},\ K_{\mathrm{li},m+1}\}\,|_{m\,=\,1,2,\ldots,N}$ values for each DG has been carried out independently through the PPOS in which the PSO stage has been run for 100 iterations with 50 particles. To conduct a comparative study, the droop relations are also designed using the CFB method in which the value of $\Delta f_{\max}$ has been set to 0.15.

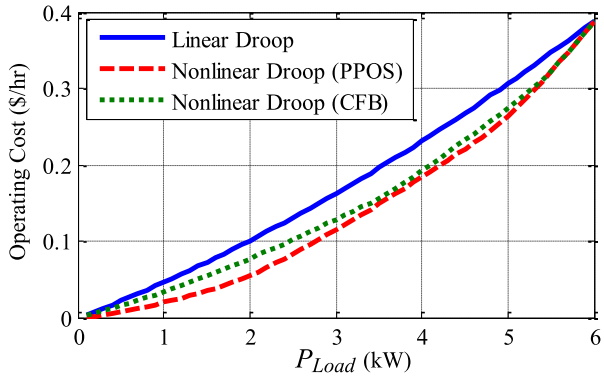

Fig. 13. Microgrid operating cost over load variation.

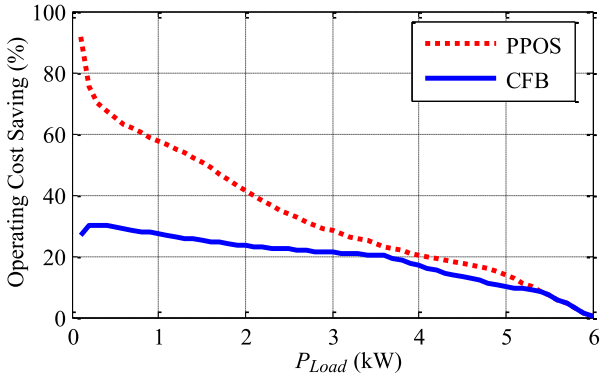

Fig. 14. Operating cost savings from the nonlinear droop relations constructed using the PPOS and the CFB methods.

Figs. 11 and 12 show the nonlinear droop relations obtained using the PPOS and the CFB methods, respectively. The power sharing among the participating DGs has been calculated based on these droop relations and the operating cost has been determined for all possible loadings to plot the total operating cost curve as shown in Fig. 13. For the conventional droop relations, an equal power sharing is considered at each loading condition due to the identical power ratings of the considered DGs. Clearly, the nonlinear droop relations obtained by the PPOS and CFB methods offer lower μG operating cost than conventional droop relations. From these calculated total operating cost data, the cost saving percentage of the PPOS and CFB methods at different loadings are plotted as shown in Fig. 14. As stated in [25], the MCB method offers 10.7%, 16.6%, and 12.6% cost savings at 25%, 50%, and 75% loadings, respectively, for the operating cost curves shown in Fig 10. As seen from Fig. 14, while the CFB method introduces better cost saving than the MCB method, the PPOS offers improved cost saving at all possible loadings compared to both existing methods. The reason of the decrease in cost savings at high loadings for all methods is that some DGs cannot contribute more to the cost savings after their saturation power.

VI. Simulation Results and Experimental Validation

In this section, the DGs in *Case Study* are considered to be effectively integrated to a μG system through its common bus

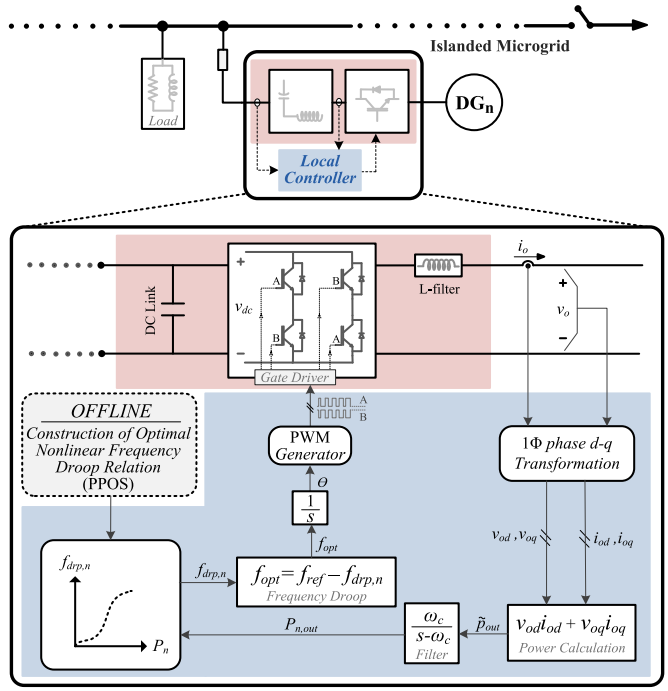

Fig. 15. Power circuit configuration and overall control block diagram of a single DG unit integrated into μG.

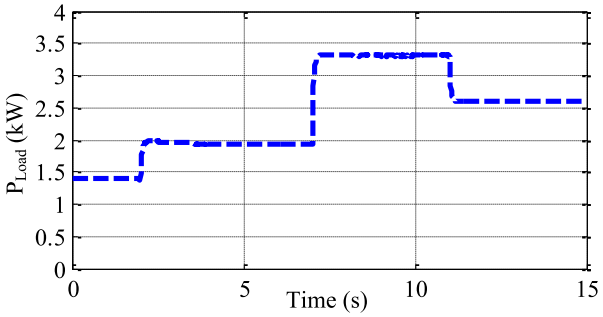

Fig. 16. Load profile used to test the cost saving performance of the nonlinear droop relations obtained from the PPOS.

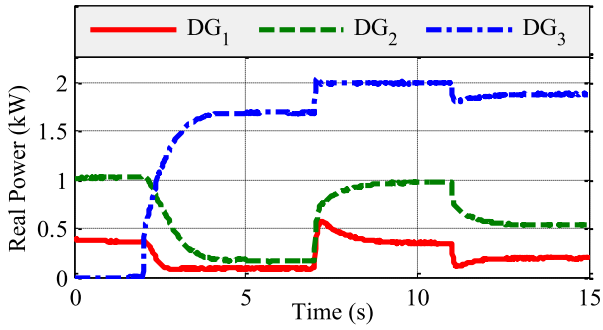

Fig. 17. Variation of real power generated by the participating DGs when controlled with the nonlinear droop relations obtained from the PPOS.

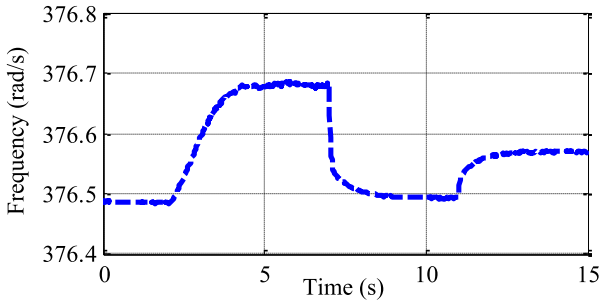

Fig. 18. Operating frequency response of the considered nonlinear droop-controlled μG corresponding to load variations.

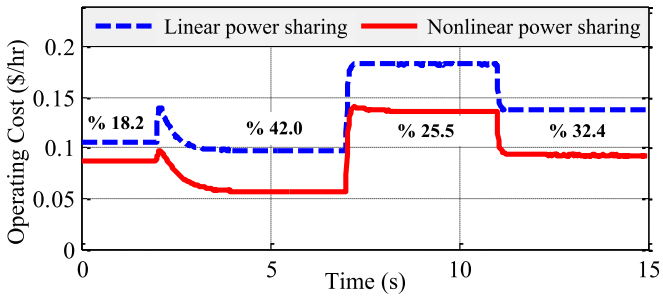

Fig. 19. Operating costs of the linear and the nonlinear droop-controlled μGs.

as shown in Fig. 15. As shown in Fig. 15, the nonlinear frequency droop control of each DG is utilized with its associated optimal nonlinear droop relation to regulate the frequency and, accordingly, perform an economical power sharing among the participating DGs. The considered μG has been simulated in MATLAB/Simulink environment with the nonlinear droop relations shown in Fig. 11 to verify the cost-saving performance of the PPOS.

To investigate the dynamic response of the nonlinear droop control and the power sharing among the DGs, the μG has been subject to load variations as shown in Fig. 16 throughout the simulation. The variations in the real output power of each DG and the μG operating frequency are shown in Figs. 17 and 18, respectively. Clearly, the DGs shares the load nonlinearly based on the constructed nonlinear droop relations and their frequency is stabilized at a certain value after each load variation applied. DG_1 and the DG_2 are initially operated together and then the DG_3 is plugged into the system after a while to also demonstrate the plug-and-play capability of the proposed method. As seen from Fig. 17, DG_1, as the most costly generator, shares the least power demand for all loading conditions because its frequency droop gain is always higher than the other DGs (see Fig. 13). On the other hand, the real power generated from the DG_3 exceeds that of the DG_1 and DG_2 for all tested loading conditions due to its relatively small frequency droop gain at all load ranges. The nonlinear droop relations obtained from the PPOS basically force the DGs introducing the least generation cost dominate the power sharing so that the μG operating cost can be minimized effectively. Fig. 19 shows the operating costs of the linear and nonlinear droop-controlled μGs and the percentage cost savings at each tested loading condition. As seen in Fig. 19, the nonlinear droop-controlled μG introduces a significant cost saving at each loading condition when it is compared with linear droop based

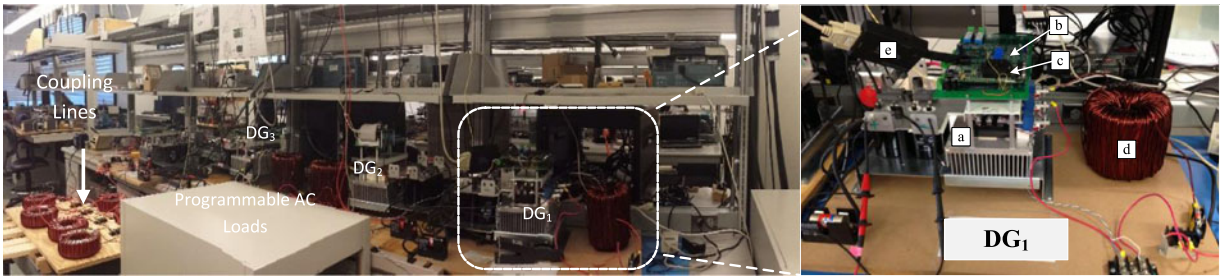

Fig. 20. Microgrid test bench: (a) Inverter unit, (b) interfacing control board, (c) DSP control board, (d) L-filter, and (e) JTAG emulator.

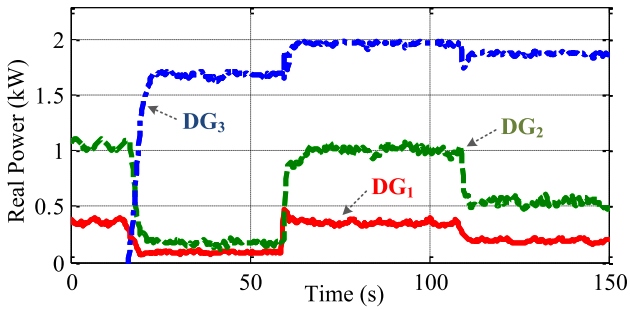

Fig. 21. Experimental results showing real powers generated by the DGs when controlled with the nonlinear droop relations obtained from the PPOS.

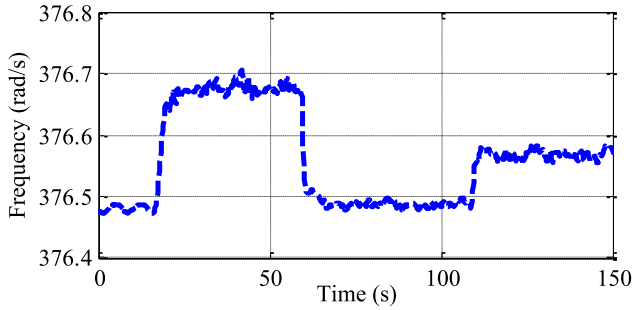

Fig. 22. Experimental results showing the operating frequency of the nonlinear droop-controlled μG corresponding to load variations.

μGs. The percentage cost saving values shown in Fig. 19 also verify the results shown in Fig. 14.

An experimental study has been conducted on a developed μG test bench (MGTB), as shown in Fig. 20, to validate the performance of the nonlinear droop control experimentally. The MGTB consists of three dc/ac inverters and each one is connected to a programmable dc supply to form a single-phase DG unit. Three DG units were connected in parallel at a common coupling point to form a μG topology similar to the simulated one. The output of each DG unit was connected to NH-research 4200 programmable ac loads so that different loading conditions could be performed. The excitation signals for controlling the inverter were provided from a DSP through an interfacing control board. Communication link between a host computer and the target DSP hardware was established by a JTAG Emulator and parallel port cable to load the control routine on the DSP and swap data throughout the experiment.

The experiment has been carried out with the same load profile used in the simulated μG topology. The optimal nonlinear droop relations shown in Fig. 11 has been implemented into the nonlinear droop control of each inverter unit using the lookup tables (LUT) in the DSP. The voltage and current signals have been measured to calculate the power produced by the DGs. This power value is first normalized and then used as an input to the LUT. The corresponding output value from the LUT has been implemented in the frequency droop. The power sharing among the participating DGs and the operating frequency variation of the considered μG are shown in Figs. 21 and 22, respectively. As expected, the experimental results are similar to the simulation results shown in Figs. 17 and 18. As seen from Fig. 21, as opposed to the case in the linear droop-controlled μG, the power sharing ratio among the DGs in the nonlinear droop-controlled μG varies subsequent to the load variation to realize minimized μG operating cost. The frequency variation shown in Fig. 22 verifies that the dynamic response of the μG operating frequency is always smoothly stabilized after each loading condition. To also verify the plug-and-play capability of the proposed method experimentally, similar to the simulation study, the DG_3 is plugged into the operating system at a certain time ($t = 16$ s) while the DG_1 and the DG_2 are online, as shown in Fig. 21. Accordingly, the performance and effectiveness of the proposed method is verified experimentally to minimize the operation cost while maintaining the smooth and stable μG operation.

VII. Conclusion

In this paper, a new method for constructing optimal nonlinear droop relation with the plug-and-play capability has been proposed to minimize the islanded microgrid operations regardless of the microgrid topology. First, the nonlinear frequency droop relations were formed as combination of power functions to satisfy the required characteristics of the droop relations and to improve the flexibility in shaping the droop relations. Then, an optimization problem was formulated based on the DG of interest against two predefined hypothetical DGs to select the determined optimal coefficients to be used in the power functions. A heuristic method, PSO, has been used as a tool to solve the defined optimization method. The results obtained in the case studies conducted in this paper clearly showed that the proposed method could improve the operation cost in

islanded microgrids when compared with the methods available in the literature. Moreover, simulation and experimental studies were conducted and their results proved that the nonlinear droop control implemented by the proposed method minimizes the operating cost while maintaining smooth stabilization in islanded μG operation.

REFERENCES

[1] International Energy Outlook 2013 Energy Information Administration, the U.S. Department of Energy Report #:DOE/EIA-0484, Jul. 2013.

[2] R. H. Lasseter, "Smart distribution: Coupled microgrids," *Proc. IEEE*, vol. 99, no. 6, pp. 1074–1082, Jun. 2011.

[3] D. Salomonsson, L. Soder, and A. Sannino, "An adaptive control network for a dc microgrid for data centers," *IEEE Trans. Ind. Appl.*, vol. 44, no. 6, pp. 1910–1917, Nov./Dec. 2008.

[4] A. Kwasinski, "Quantitative evaluation of dc microgrids availability: Effects of network architecture and converter topology design choices," *IEEE Trans. Power Electron.*, vol. 26, no. 3, pp. 835–851, Mar. 2011.

[5] N. Bottrell, M. Prodanovic, and T. C. Green, "Dynamic stability of a microgridwith an active load," *IEEE Trans. Power Electron.*, vol. 28, no. 11, pp. 5107–5119, Nov. 2013.

[6] Y.-K. Chen, Y.-C. Wu, C.-C. Song, and Y.-S. Chen, "Design and implementation of energy management network with fuzzy control for dc microgrid networks," *IEEE Trans. Power Electron.*, vol. 28, no. 4, pp. 1563–1570, Apr. 2013.

[7] N. Hatziargyriou, H. Asano, R. Iravani, and C. Marnay, "Microgrids," *IEEE Power Energy Mag*., vol. 5, no. 4, pp. 78–94, Jul.–Aug. 2007.

[8] R. H. Lasseter, "Certs microgrid," in *Proc. IEEE SoSE*, pp. 1–5, Apr. 2007.

[9] H. Nikkhajoei and R. H. Lasseter, "Distributed generation interface to the CERTS microgrid," *IEEE Trans. Power Del.*, vol. 24, no. 3, pp. 1598–1608, Jul. 2009.

[10] P. C. Loh, D. Li, Y. Chai, and F. Blaabjerg, "Autonomous operation of hybrid microgrid with ac and dc subgrids," *IEEE Trans. Power Electron.*, vol. 28, no. 5, pp. 2214–2223, May 2013.

[11] J. Guerrero, J. C. Vasquez, and L. G. D. Vicuna, "Hierarchical control of droop-controlled AC and DC microgrids—A general approach toward standardization," *IEEE Trans. Ind. Electron.*, vol. 58, no. 1, pp. 158–172, Jan. 2011.

[12] T. L. Vandoorn, J. C. Vasquez, J. D. Kooning, J. M. Guerrero, and L. Vandevelde, "Microgrids: Hierarchical control and an overview of the control and reserve management strategies," *IEEE Ind. Electron. Mag*, vol. 7, no. 4, pp. 42–55, Dec. 2013.

[13] J. A. P. Lopes, C. L. Moreira, and A. G. Madureira, "Defining control strategies for microgrids islanded operation," *IEEE Trans. Power Syst.*, vol. 21, no. 2, pp. 916–924, May 2006.

[14] M. C. Chandorkar, D. M. Divan, and R. Adapa, "Control of parallel connected inverters in standalone AC supply networks," *IEEE Trans. Ind. Appl.*, vol. 29, no. 1, pp. 136–143, 1993.

[15] K. Jaehong, J. M. Guerrero, P. Rodriguez, R. Teodorescu, and N. Kwanghee, "Mode adaptive droop control with virtual output impedances for an inverter-based flexible AC microgrid," *IEEE Trans. Power Electron*, vol. 26, no. 3, pp. 689–701, 2011.

[16] F. Katiraei, M. R. Iravani, and P. W. Lehn, "Microgrid autonomous operation during and subsequent to islanding process," *IEEE Trans. Power Del.*, vol. 20, no. 1, pp. 248–257, 2005.

[17] S. Anand, B. G. Fernandes, and J. M. Guerrero, "Distributed control to ensure proportional load sharing and improve voltage regulation in low-voltage DC microgrids," *IEEE Trans. Power Electron.*, vol. 28, no. 4, pp. 1900–1913, 2013.

[18] J. M. Guerrero, P. Loh, M. Chandorkar, and T. Lee, "Advanced control architectures for intelligent microgrids—Part I: Decentralized and hierarchical control," *IEEE Trans. Ind. Electron.*, vol. 60, no. 4, pp. 1254–1262, 2012.

[19] J. Vasquez, J. M. Guerrero, M. Savaghebi, J. Eloy-Garcia, and R. Teodorescu, "Modeling, analysis, and design of stationary reference frame droop controlled parallel three-phase voltage source inverters," *IEEE Trans. Ind. Electron.*, vol. 60, no. 4, pp. 1271–1280, 2013.

[20] A. Bidram and A. Davoudi, "Hierarchical structure of microgrids control network," *IEEE Trans. Smart Grid*, vol. 3, no. 4, pp. 1963–1976, Dec. 2012.

[21] C. A. Hernandez-Aramburo, T. C. Green, and N. Mugniot, "Fuel consumption minimization of a microgrid," *IEEE Trans. Ind. Appl.*, vol. 41, no. 3, pp. 673–681, May-Jun. 2005.

[22] I. U. Nutkani, P. C. Loh, P. Wang, and F. Blaabjerg, "Autonomous droop scheme with reduced generation cost," *IEEE Trans. Ind. Electron.*, vol. 61, no. 12, pp. 6803–6811, Dec. 2014.

[23] I. U. Nutkani, P. C. Loh, and F. Blaabjerg, "Droop scheme with consideration of operating costs," *IEEE Trans. Power Electron.*, vol. 29, no. 3, pp. 1047–1052, Mar. 2014.

[24] I. U. Nutkani, P. C. Loh, and F. Blaabjerg, "Cost-based droop scheme with lower generation costs for microgrids," *IET Power Electron*., vol. 7, no. 5, pp. 1171–1180, May 2014.

[25] I. Nutkani, P. Loh, P. Wang, and F. Blaabjerg, "Linear decentralized power sharing schemes for economic operation of AC microgrids," *IEEE Trans. Ind. Electron.*, vol. 63, no. 1, pp. 225–234, Aug. 2015.

[26] A. Elrayyah and Y. Sozer, "Construction of nonlinear droop relations to optimize islanded microgrids operation," in *Proc. IEEE Energy Convers. Congr. Expo.*, Sep. 15–19, 2013, pp. 1663–1668.

[27] A. Elrayyah, F. Cingoz, and Y. Sozer, "Construction of nonlinear droop relations to optimize islanded microgrids operation," *IEEE Trans. Ind. Appl.*, vol. 51, no. 4, pp. 3404–3413, Jul.–Aug. 2015.

[28] I. Nutkani, P. Loh, P. Wang, and F. Blaabjerg, "Cost-prioritized droop schemes for autonomous AC microgrids," *IEEE Trans. Power Electron.*, vol. 30, no. 2, pp. 1109–1119, Feb. 2015.

[29] I. Nutkani, P. Loh, P. Wang, and F. Blaabjerg, "Decentralized economic dispatch scheme with online power reserve for microgrids," *IEEE Trans. Smart Grid*, to be published.

[30] A. Mehrizi-Sani and R. Iravani, "Potential function based control of a microgrid in islanded and grid-connected modes," *IEEE Trans. Power Syst.*, vol. 25, no. 4, pp. 1883–1891, Nov. 2010.

[31] K. D. Brabandere, K. Vanthournout, J. Driesen, G. Deconinck, and R. Belmans, "Control of microgrids," in *Proc. IEEE Power Energy Soc. Gen. Meeting*, pp. 1–7, Jun. 2007.

[32] H. Nikkhajoei and R. H. Lasseter, "Distributed generation interface to the CERTS microgrid," *IEEE Trans. Power Del.*, vol. 24, no. 3, pp. 1598–1608, Jul. 2009.

[33] H. Karimi, H. Nikkhajoei, and M. R. Iravani, "Control of an electronically-coupled distributed resource unit subsequent to an islanding event," *IEEE Trans. Power Del.*, vol. 23, no. 1, pp. 493–501, Jan. 2008.

[34] P. C. Loh, D. Li, Y. K. Chai, and F. Blaabjerg,, "Hybrid AC–DC microgrids with energy storages and progressive energy flow tuning," *IEEE Trans. Power Electron*, vol. 28, no. 4, pp. 1533–1543, Apr. 2013.

[35] J. He, Y. W. Li, J. M. Guerrero, F. Blaabjerg, and J.C. Vasquez, "An islanding microgrid power sharing approach using enhanced virtual impedance control scheme," *IEEE Trans. Power Electron.*, vol. 28, no. 11, pp. 5272–5282, Nov. 2013.

[36] Q. Shafiee, J. M. Guerrero, and J. C. Vasquez, " Distributed secondary control for islanded microgrids A novel approach," *IEEE Trans. Power Electron.*, vol. 29, no. 2, pp. 1018–1031, Feb. 2014.

[37] J. He, Y. W. Li, J. M. Guerrero, F. Blaabjerg, and J. C. Vasquez, "An islanding microgrid power sharing approach using enhanced virtual impedance control scheme," *IEEE Trans. Power Electron.*, vol. 28, no. 11, pp. 5272–5282, Nov. 2013.

[38] D. Wu, F. Tang, G. J. M. Vasquez, J. C. G. Chen, and L. Sun, "Autonomous active and reactive power distribution strategy in islanded microgrids," in *Proc. Appl. Power Electron. Conf. Exp.*, 2014, pp. 2126–2131.

[39] X. Zhang, J. Liu, and T. Liu, "Virtual negatively resistive output impedance for power sharing among paralleled inverters in microgrid," in *Proc. 2011 IEEE 8th Int. Conf. Power Electron. ECCE Asia,* pp. 1809–1812.

[40] A. Yazdani and M. Delghavi, "An adaptive feedforward compensation for stability enhancement in droop-controlled inverter-based microgrids," *IEEE Trans. Power Del.*, vol. 26, no. 3, pp. 1764–1773, Jul. 2011.

[41] J. Kim, J. M. Guerrero, P. Rodriguez, R. Teodorescu,∗∗∗ and K. Nam, "Mode adaptive droop control with virtual output impedances for an inverter-based flexible AC microgrid," *IEEE Trans. Power Electron.*, vol. 26, no. 3, pp. 689–701, Mar. 2011.

[42] R. H. Lasseter, "Microgrids," in *Proc. IEEE Power Eng. Soc. Winter Meeting*, 2002, pp. 305–308.

[43] G. Binetti, A. Davoudi, F. L. Lewis, D. Naso, and B. Turchiano, "Distributed consensus-based economic dispatch with transmission losses," *IEEE Trans. Power Syst.*, vol. 29, no. 4, pp. 1711–1720, Jul. 2014.

[44] G. Binetti, A. Davoudi, D. Naso, B. Turchiano, and F. L. Lewis, "A distributed auction-based algorithm for the nonconvex economic dispatch problem," *IEEE Trans. Ind. Inform.*, vol. 10, no. 2, pp. 1124–1132, May 2014.

[45] A. Bidram, A. A. Davoudi, and F. L. Lewis, "A multi-objective distributed control framework for islanded ac microgrids," *IEEE Trans. Ind. Inform.*, vol. 10, no. 3, pp. 1785–1798, May 2014.
[46] H. Liang, B. J. Choi, A. Abdrabou, W. Zhuang, and X. S. Shen, "Decentralized economic dispatch in microgrids via heterogeneous wireless networks," *IEEE J. Select. Areas Commun.*, vol. 30, no. 6, pp. 1061–1074, Jul. 2012.
[47] K. Y. Lee and M. A. El-Sharkawi, *Modern Heuristic Optimization Techniques: Theory and Applications to Power Systems*. Hoboken, NJ, USA: IEEE Press/Wiley-Interscience, 2008.
[48] J. Kennedy and R. Eberhart, "Particle swarm optimization," in *Proc. IEEE. Int. Conf. Neural Netw.* Nov./Dec. 1995, vol. 4, pp. 1942–1948.
[49] M. S. Branicky,"Multiple Lyapunov functions and other analysis tools for switched and hybrid systems," *IEEE Trans. Autom. Contr.*, vol. 43, no. 4, pp. 475–482, Apr. 1998.
[50] D. Liberzon and A. S. Morse, "Basic problems in stability and design of switched systems," *IEEE Cont. Syst. Mag.*, vol. 19, no. 5, pp. 59–70, Oct. 1999.

Fatih Cingoz (S'12) received the B.S. degree from Selcuk University, Konya, Turkey, in 2008, and the M.S. degree from the University of Texas at Arlington, Arlington, TX, USA, in 2012, all in electrical engineering. He is currently working toward the Ph.D. degree at the University of Akron, Akron, OH, USA.

His current research interests include renewable and sustainable energy systems and control of microgrids.

Ali Elrayyah (M'15) received the B.Sc. degree in electrical and electronics engineering from the University of Khartoum, Khartoum, Sudan, in 2003, the M.Sc. degree in systems engineering from King Fahd University of Petroleum and Minerals (KFUPM), Dhahran, Saudi Arabia, in 2009, and the Ph.D. degree from University of Akron, Akron, OH, USA, in 2013.

He is currently a Research Engineer at the Qatar Research Foundation, Doha, Qatar. His research interests include alternative energy systems, and control of standalone and utility interactive energy systems.

Yilmaz Sozer (M'05–SM'14) received the B.S. degree in electrical engineering from the Middle East Technical University Ankara, Ankara, Turkey, and the M.S. and Ph.D. degrees in electric power engineering from Rensselaer Polytechnic Institute Troy, Troy, NY, USA.

He was involved in power electronics and the development of control algorithms for electric machines. He is currently an Associate Professor in the Electrical and Computer Engineering Department, University of Akron, where he is engaged in teaching and research. Before joining the University of Akron, he was with Advanced Energy Conversion Schenectady, NY. His current research interests include in the areas of control and modeling of electrical drives, alternative energy systems, design of electric machines, high-power isolated dc/dc converter systems, static power conversion systems that interface energy storage, and distributed generation sources with the electric utility.

Dr. Sozer has been involved in IEEE activities which support power electronics, electric machines, and alternative energy systems. He is an Associate Editor of the IEEE TRANSACTIONS ON INDUSTRY APPLICATIONS and the IEEE TRANSACTIONS ON POWER ELECTRONICS. He is a Vice Chair for the IEEE IAS Renewable and Sustainable Energy Conversion Systems Committee.